Journal of Biomedical Optics

BiomedicalOptics.SPIEDigitalLibrary.org

Assessment of asthmatic inflammation using hybrid fluorescence molecular tomography–x-ray computed tomography

Xiaopeng Ma
Jaya Prakash
Francesca Ruscitti
Sarah Glasl
Fabio Franco Stellari
Gino Villetti
Vasilis Ntziachristos

SPIE.

Assessment of asthmatic inflammation using hybrid fluorescence molecular tomography–x-ray computed tomography

Xiaopeng Ma,[a,b] Jaya Prakash,[a,b] Francesca Ruscitti,[c] Sarah Glasl,[a,b] Fabio Franco Stellari,[d] Gino Villetti,[d] and Vasilis Ntziachristos[a,b,*]

[a]Helmholtz Zentrum München, Institute for Biological and Medical Imaging, Ingolstaedter Landstrasse 1, Neuherberg, D-85746, Germany
[b]Technische Universität München, Chair for Biological Imaging, Ismaninger Street 22, Munich 81675, Germany
[c]University of Parma, Department of Biomedical, Biotechnological and Translational Science, via del Taglio 10, Parma, 43126, Italy
[d]Corporate Pre-clinical R&D, Chiesi Farmaceutici S.p.A, Largo Francesco Belloli 11/A, Parma, 43122, Italy

Abstract. Nuclear imaging plays a critical role in asthma research but is limited in its readings of biology due to the short-lived signals of radio-isotopes. We employed hybrid fluorescence molecular tomography (FMT) and x-ray computed tomography (XCT) for the assessment of asthmatic inflammation based on resolving cathepsin activity and matrix metalloproteinase activity in dust mite, ragweed, and *Aspergillus* species-challenged mice. The reconstructed multimodal fluorescence distribution showed good correspondence with *ex vivo* cryosection images and histological images, confirming FMT-XCT as an interesting alternative for asthma research. [DOI: 10.1117/1.JBO.21.1.015009]

Keywords: multimodality imaging; fluorescence molecular tomography; x-ray computed tomography; asthmatic inflammation; dust mite, ragweed, and *Aspergillus* species-challenged mouse model.

Paper 150734R received Oct. 31, 2015; accepted for publication Dec. 15, 2015; published online Jan. 21, 2016.

1 Introduction

Asthma is a chronic lung disease affecting millions of people across the world. Bronchial hyper-responsiveness (BHR), airway inflammation, and airway remodeling are key symptoms that characterize the disease.[1–4] Chronic airway inflammation involves recruitment of inflammatory cells, such as T lymphocytes, mast cells, and eosinophils. Among all asthma-related inflammatory cells, eosinophils are predominant and are well known to produce various proteases in asthma, including cathepsins B, S, L, H, and K, which are thought to contribute to the pathogenesis of the asthma disease.[5,6] Cathepsin activity has been employed as a biomarker of disease severity in asthma models using near-infrared fluorescent agents.[7] Remodeling is commonly believed to occur as a result of pathological repair of an airway chronic inflammation process.[8] The airway chronic inflammation involves structural changes in the airway's architecture in asthmatic patients, such as airway narrowing, wall thickening which results in airflow obstruction, and persistent BHR. The complex mechanisms behind the remodeling process are not fully understood.[9] Nevertheless, matrix metalloproteinases (MMPs) have been identified as enzymes that are synthesized and produced by inflammatory cells and resident cells[10] and capable of degrading the extracellular matrix, thus playing a critical role in remodeling.[11,12] Elevated MMP expression has been associated with airway inflammation and remodeling.[12]

The *in vivo* study of asthma and related drugs commonly involves mouse models.[13] Animal measurements, however, face limitations. A common drawback of many mouse models is that the animals develop tolerance when exposed to the same allergen.[14] In this case, an asthma phenotype reaches a peak in 2 or 3 days after a challenge, but the biological response drastically reduces within 1 to 2 weeks. To improve on this limitation, Goplen et al.[15] have described an animal model of asthma that sustains the disease phenotype for at least 3 weeks by sensitizing mice with a combination of three allergens relevant for human pathology: dust mite, ragweed, and *Aspergillus* species (DRA).[15] In addition to sustaining asthma-related inflammatory responses over time, the DRA mouse model has the capability to sustain asthmatic features even after discontinuation of exposure to allergens.[15]

The second limitation of small animal asthma research has been the ability to retrieve accurate longitudinal measurements of disease biomarkers. Traditionally, histological studies used for evaluation of bronchial inflammation, airway obstruction, and remodeling involve animal sacrifice, which only allows measurements at single time points. The requirement to assess disease progression or response to treatment has shifted attention to noninvasive technologies.[16] Spirometry is a long-known noninvasive technique[17] that estimates asthma severity by measuring the inhaled and exhaled air volume[17] but can result in overestimation and measurement uncertainty.[18] X-ray computed tomography (XCT) is a commonly used imaging modality to assess airway remodeling.[19–21] XCT identifies anatomical changes but cannot visualize biological parameters associated with pulmonary inflammation.[22] Nuclear medicine is a noninvasive functional imaging technique used for asthma research.[23] Nuclear medicine provides good functional information but suffers from short-lived signals of the radio-isotopes.[24]

Optical methods have also been considered for asthma research. A limitation with commonly employed fluorescence

*Address all correspondence to: Vasilis Ntziachristos, E-mail: v.ntziachristos@tum.de

1083-3668/2016/$25.00 © 2016 SPIE

epi-illumination imaging is that it is sensitive to surface fluorescence activity and cannot reliably visualize signals in the lung.[25] Transillumination and tomographic techniques, in particular, fluorescence molecular tomography (FMT), have been proved more efficient for sampling biological processes in pulmonary diseases compared to epi-illumination fluorescence imaging.[7,26,27] The ability to visualize pulmonary inflammation has been demonstrated using a limited-angle FMT system in animal models of chronic obstructive pulmonary disease (COPD).[28] Conversely, standalone FMT is unable to provide high-fidelity functional information due to strong photon scattering in tissue and the corresponding ill-posed nature of the inversion problem.[29,30] The recent development of hybrid imaging employing FMT and XCT under a common rotating gantry has shown significant improvements in the resolution and quantification achieved by the optical method.[31] The hybrid modality utilizes the XCT information for anatomical coregistration with the fluorescence images, allowing better orientation of the biological signals in relation to morphological landmarks.[31–33] Importantly, however, the XCT information is also employed as prior information into the FMT inverse problem, improving the overall accuracy and resolution by reducing the ill-posed nature of the inverse problem.[31,34–36] Compared to previous FMT studies using limited angle projection illumination,[28] FMT-XCT further provides 360-deg angle coverage, further improving the imaging fidelity. However, there has been no systematic evaluation of FMT-XCT in its ability to resolve asthma biomarkers in animal models. In this work, we hypothesized that FMT-XCT could be ideally suited for asthma research studies due to its unique ability to combine anatomical and fluorescence-based biological contrast. In particular, we investigated the performance of FMT-XCT in measuring pulmonary eosinophilias and MMP activity in a DRA mouse model.

2 Materials and Methods

2.1 *Mouse Model and Imaging Agents*

Among the large number of murine asthma models present in the literature, the DRA chronic asthma model was chosen, since it maintains eosinophilic inflammation, remodeling, and other features of asthma for at least 3 weeks of exposure to allergens.[15] Female Balb-C mice (7 to 8 weeks old) were purchased from The Harlan Laboratories (Indianapolis, Indiana). For asthmatic groups, each mouse received an intranasal administration of 15 μL volume of DRA allergen solution twice a week, using a 200-μL pipette to reproduce the biological and molecular features of human chronic asthma. The 15-μL DRA mixture solution was prepared using a 5-μg dust mite in 5 μL (extracts of *Dermatophagoides farinae*, Greer Laboratories, North Carolina), 50 μg ragweed in 5 μL (extracts of *Ambrosia artemisiifolia*, Greer Lab), and 5 μg *Aspergillus* in 5 μL (extracts of *Aspergillus fumigatus*, Greer Lab). Three experimental animal groups were established by means of DRA exposure, namely, DRA exposure for 6 weeks, 9 weeks, and 9 weeks followed by 3 weeks of rest (12-week group). The control group received 15 μL of saline using the same intranasal administration.

Two different commercially available near-infrared imaging agents, namely ProSense680 (Perkin Elmer, Waltham, Massachusetts) activated by Cathepsin B and MMPSense680 (Perkin Elmer, Waltham, Massachusetts) activated by MMPs, were intravenously administered prior to imaging studies. The excitation and emission wavelengths of both imaging agents are approximately at 680/700 nm. Around 2 nmol of near-infrared imaging agent was injected into each mouse 24 h prior to FMT-XCT *in vivo* imaging. The quantity of the injected imaging agent was calculated based on the body weight of the mouse. The ProSense680 dosage was given to the mouse at week 6 and week 9, while the mice were injected with MMPSense680 at week 12. For the ProSense680 group, 10 mice were used (three for control, three for week 6, and four for week 9). For the MMPSense680 group, six mice were imaged (two for control and four for week 12).

2.2 *Fluorescence Molecular Tomography and X-Ray Computed Tomography and Cryoslicing*

FMT-XCT was performed on a home-built system previously employed for bone remodeling and cancer studies in small animals.[31,37] The system employs a 360-deg rotation gantry system carrying both the XCT and the FMT illumination and detection components to achieve hybrid imaging of mice under identical placement conditions. To avoid fluorescent signal from food, all mice were fed a nonfluorescent diet before starting the experiments and during the whole experimental process. Mice were first shaved and chemically depilated to reduce the influence of the fur on the optical measurements. Then animals were anesthetized by isoflurane inhalation (isoflurane 2.5%, O_2 0.85 L/min) during the imaging experiment. Quantitative three-dimensional (3-D) fluorophore distribution was reconstructed using the least squares QR[38] technique with 50 iterations. Mean values of the fluorescence distribution were computed in the thorax region (obtained by the XCT transverse image).

After FMT-XCT imaging, the mice were euthanized, frozen to −50°C, and submitted for whole-body cryoslicing. Fluorescence images were acquired from the mouse cryoslices and were employed for validation of the *in vivo* findings. All cryoslicing imaging were performed by the multispectral epi-illumination cryoslicing home-built imaging system.[39] *Ex vivo* cryoslicing (considered as a "gold standard") offers high-resolution colored and fluorescent cross-sectional images of the animal lung. A maximum exposure time of 7 s was applied to acquire the cryosection fluorescence images. The mean fluorescence intensity value in the lung region of each slice of the fluorescent cyrosection image was quantified. The quantification procedure involved normalizing the fluorescence image by the exposure time after background subtraction. The background subtraction was executed by choosing a 200×200 pixel region of the image that did not contain mouse tissue and calculating the mean value of this region. This background mean value was then subtracted from the whole fluorescent cryosection image. After normalization, specific regions of interest (ROI) were extracted from the color image and were used to compute the mean intensity of the fluorescence image in the ROI (note that the color and fluorescence images were obtained using same parameters). Last, main slices in the lung region were marked and processed by the above procedure to compute the average fluorescence intensity value for these marked slices.

All *in vivo* studies and procedures were approved by Helmholtz Zentrum München and the District Government of Upper Bavaria.

2.3 *H&E Staining of Lung Tissue*

For H&E staining, the ROI slices were fixed in 4% PFA (Santa Cruz, Heidelberg) and then rinsed with distilled water. To stain

the nuclei, the slices were incubated in Mayer's hematoxylin (Carl Roth, Karlsruhe, Germany) for 30 s and then rinsed with tap water, which changed the color from red to blue due to the pH change. To stain the cytoplasm, the slices were incubated in eosin G (Carl Roth, Karlsruhe, Germany) for 1 s and rinsed with distilled water. For the next step, slices were dehydrated in 70%, 94%, and 100% ethanol, followed by 10 min xylene incubation. At a last step, the slices were covered with Rotimount cover media (Carl Roth, Karlsruhe, Germany). Representative slides were observed using a Zeiss Axio Imager M2 upright microscope, and pictures were taken using a color Axiocamera 105 Color (Carl Zeiss, Jena, Germany).

3 Results

3.1 *Quantitative Evaluation of Asthma-Related Inflammation Using ProSense680*

Figure 1 shows results from the *in vivo* studies and *ex vivo* validations. Figure 1 compares hybrid FMT-XCT reconstruction results with fluorescent cryosection images for two mice in week 6 using ProSense680 as imaging agent. One of the mice acts as a control (first row of Fig. 1), while the other mouse is DRA-sensitized for 6 weeks (second row of Fig. 1). Figure 1(a) shows a transverse XCT cross section through the lung region of the control (which was intranasally treated with saline for 6 weeks). The reconstructed fluorescence signal is superimposed on the transverse XCT cross section as shown in Fig. 1(b). Corresponding *ex vivo* color and fluorescence images of the control mouse were obtained by cryoslicing and are shown in Figs. 1(c) and 1(d), respectively; these cryoslicing images are used for validation of FMT-XCT reconstructions. Figures 1(e)–1(h) show the *in vivo* and *ex vivo* images for the 6 week DRA-sensitized asthma mouse model. White arrows in Figs. 1(e)–1(h) indicate the same region in the ROI, demonstrating one mild inflammatory part in the left lung. Comparison between the lung regions of Figs. 1(d) and 1(h) indicates a higher fluorescence intensity can be found in the asthmatic mouse from cryoslicing. The comparison of the FMT-XCT reconstructed fluorescence distribution between the control mouse and the DRA-challenged mouse also clearly indicates an increase in fluorescence signal in the lung region [refer to Figs. 1(b) and

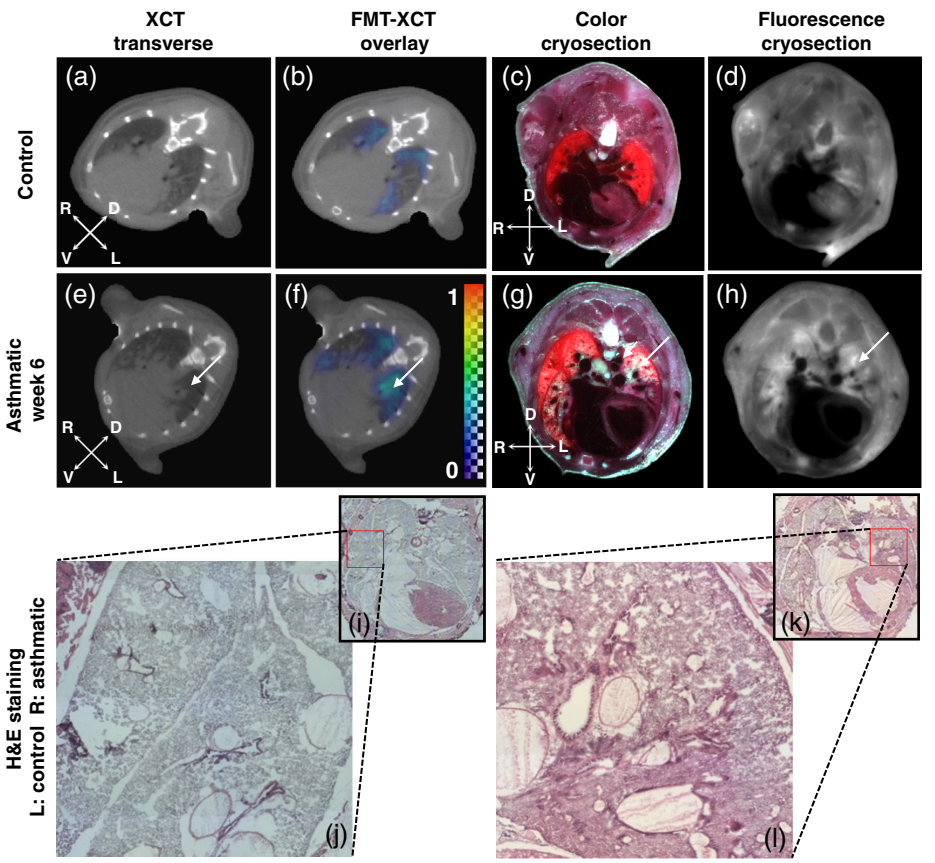

Fig. 1 One representative slice comparison of FMT-XCT reconstruction, cryoslicing image, and H&E staining in sixth week using ProSense680 as the fluorescent agent between control mouse and asthmatic mouse models. (a)–(d) Images obtained from different imaging modalities for the same slice of a control mouse in the sixth week. (a) XCT transverse plane, (b) transverse slice of FMT reconstruction overlaid on XCT slice, (c) cryoslicing color image, (d) transverse-normalized fluorescent cryosection for validation of FMT-XCT reconstruction. (e)–(h) Images obtained from different imaging modalities of DRA-sensitized asthma mice in the sixth week. (e) XCT transverse plane, (f) transverse slice of FMT reconstruction overlaid on XCT slice, (g) cryoslicing color image, (h) transverse-normalized fluorescent cryosection. (i) and (j) H&E staining result of control mouse, (i) whole sample slide, (j) larger picture of the red rectangular region in (i). (k) and (l) H&E staining result of asthmatic mouse at the same time point, (k) whole sample slide, (l) shows a larger figure of the red rectangular region in (k). Coordinate systems are designated by D (dorsal), V (ventral), L (left), and R (right).

1(f)]. The cryosliced fluorescence profile and hybrid FMT-XCT reconstruction were found to have considerable correspondence as shown in Fig. 1. The arrows in Figs. 1(f) and 1(h) indicate the part of lung having a high fluorescence signal, indicative of asthma-related biological activity. Note that due to the process of freezing and small displacements of the animals, small shifts between *in vivo* images and *ex vivo* cryoslicing images are expected, and hence totally identical representations cannot be achieved. Figures 1(i)–1(l) show the H&E staining images; asthmatic features can be clearly observed in the 6 weeks DRA-treated mouse compared to the control mouse [refer to Figs. 1(j) and 1(l)]. These asthmatic features represent significant inflammatory infiltration and airway epithelium hypertrophy. This biologic finding is very well correlated with the FMT-XCT reconstruction results.

Figure 2 shows FMT-XCT reconstructions along with cryoslicing images for both the control mouse and asthma mouse model in week 9 using ProSense680 as imaging agent. Figures 2(a)–2(d) show images obtained from *in vivo* FMT-XCT experiments and *ex vivo* cryoslicing of the control mouse at week 9. Figure 2(a) shows the transverse plane of the XCT image, and Fig. 2(b) shows the FMT-XCT reconstructed fluorescence signal overlaid over the transverse XCT slice. Figure 2(c) indicates a color cryoslicing image of the control mouse while Fig. 2(d) represents the corresponding fluorescence cryosection after normalization with exposure time and background subtraction. Figures 2(e)–2(h) indicate results of the DRA-challenged asthma model in week 9. Fluorescence accumulation in the lung region was observed clearly in Fig. 2(f), which correlated well with the cryosection image in Fig. 2(h); all the white arrows in Fig. 2 highlight the strongest inflammatory regions. As observed from Fig. 2, the FMT-XCT imaging technique achieved good conformity with the cryosection validation results. The inflammatory lung regions were fairly distinguishable from surrounding tissue [see Figs. 2(f) and 2(h)]. After 9 weeks of DRA treatment, more severe inflammatory cell accumulation was

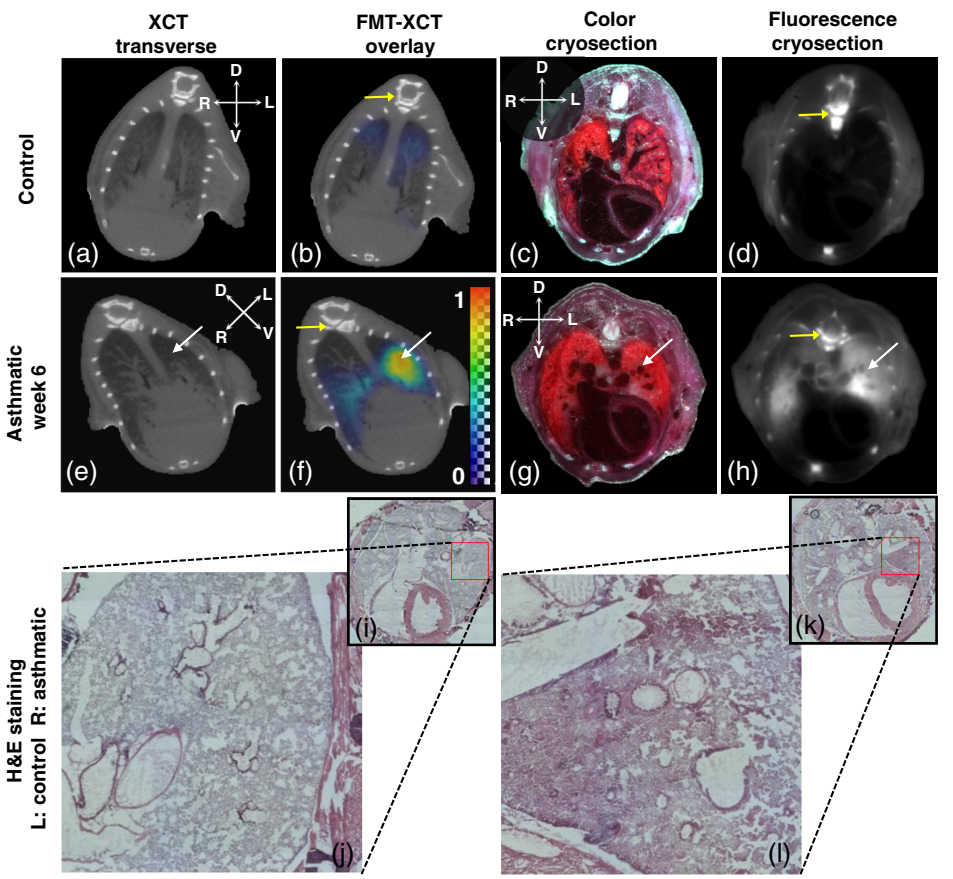

Fig. 2 Representative slice comparison of FMT-XCT reconstruction, cryoslicing images, and H&E staining in week 9 using ProSense680 as the fluorescent agent. (a)–(d) Images obtained from different imaging modalities of the same slice of one control mouse. (a) XCT transverse plane, (b) transverse slice of FMT reconstruction overlaid on XCT slice, (c) cryoslicing color image, (d) transverse-normalized fluorescent cryosection. (e)–(h) Images obtained from different imaging modalities of the same slice of DRA-sensitized asthma murine tissue at time point of 9 weeks. (e) XCT transverse plane, (f) transverse slice of FMT reconstruction overlaid on XCT slice, (g) cryoslicing color image, (h) transverse-normalized fluorescent cryosection for validation of FMT reconstruction. All white arrows illustrate the same region in ROI, indicating the most serious inflammatory part in the lung of the asthmatic mouse. (i) and (j) H&E staining result of control mouse in week 9. (i) Whole sample slide. Enlarged view (j) represents the red rectangular region in (i). (k) and (l) H&E staining result of DRA-challenged asthmatic mouse in week 9. (k) Whole sample slide. Enlarged view (l) represents the red rectangular region in (k). Coordinate systems are designated by D (dorsal), V (ventral), L (left), and R (right).

observed compared to control mouse. Note that the severity was also much higher compared to the week 6 analysis, making FMT-XCT very useful in the staging of asthma. The severity can be seen by multiple lung lobe impairment, with a loss of the alveolar segment. These challenged areas are all found associated with the bronchus, or middle-sized airways, indicating one intratracheal-treated tissue damage. The involved lobes also showed a high fluorescence signal in our FMT-XCT reconstruction analysis and corresponding cyrosection slide. Fluorescence signals were also observed in the bone region in both Figs. 2(d) and 2(h), which also demonstrates the important role of cathepsins in bone resorption.[40] Usage of the prior XCT-based segmentation information in the FMT-XCT reconstruction allows us to discard the artifacts along with the false-positive signals from ribs in Figs. 2(b) and 2(f). As indicated by yellow arrows in Figs. 2(d) and 2(h), high fluorescence signal could be seen in mouse's spine region from cryoslicing fluorescence images. However, the corresponding FMT-XCT reconstruction results indicate much less fluorescence concentration at the mouse's spine region [see Figs. 2(b) and 2(f)].

Figure 3 depicts a 3-D rendered image of mouse bones and lungs coregistered with fluorescence intensity acquired from FMT-XCT reconstructions and fluorescent cryosections, respectively, for two different time points of the DRA model and control one. Figures 3(a) and 3(d) depict the same control mouse. Figures 3(b) and 3(e) represent the FMT-XCT reconstruction and cryosections for the 6 weeks DRA-sensitized mouse, while Figs. 3(c) and 3(f) indicate the same for the 9 weeks DRA-sensitized mouse. The 3-D renderings offer a direct assessment of the volumetric activity present in the lung and similarly showcase increased activity in the entire DRA-sensitized organ compared to the control lung.

3.2 *Quantitative Evaluation of Asthma-Related Inflammation and Remodeling Using MMPSense680*

Analysis of different airway parameters in the chronic DRA model has shown that 3 weeks after the last DRA challenge, the airway inflammation and remodeling is persistent.[15] Previous studies also showed MMP activity can be effective for assessing the severity of pulmonary inflammation and remodeling.[26] The ability of the hybrid FMT-XCT system to resolve parameters in evaluating asthma-related inflammation and remodeling by the fluorescent agent MMPSense680 is examined. Here, six mice were imaged with FMT-XCT along with cryoslicing validation; two of these mice act as controls while four mice were challenged for 9 weeks and rested for 3 weeks.

Figure 4 shows the results of *in vivo* and *ex vivo* studies from week 12 (3 weeks after last DRA challenge in week 9), intravenously injected with MMPSense680. Comparisons of the control and asthmatic mouse on a representative transverse slice of the XCT image are shown in Figs. 4(a) and 4(e), respectively. The comparisons of the FMT reconstruction overlaid on the XCT with the representative slice for the control and asthmatic mouse are shown in Figs. 4(b) and 4(f), respectively. Figures 4(c) and 4(g) show the color cryosection images of the same slice with control and asthmatic mouse, respectively, while Figs. 4(d) and 4(h) show the corresponding fluorescence cryosection images. The first row in Fig. 4 indicates one representative control mouse which was intranasally treated with saline for 9 weeks and rested for 3 weeks. The second row shows a mouse treated with 9 weeks of DRA challenge and rested for 3 weeks after the challenge. Arrows in Figs. 4(f) and 4(h) indicate a clear increase in the fluorescence distribution compared to nearby lung tissue, indicating the capability of

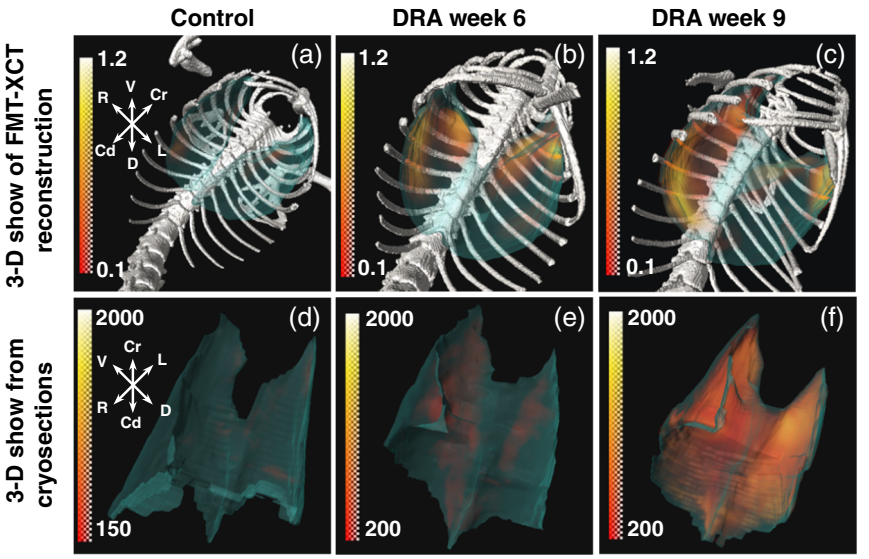

Fig. 3 3-D rendering comparison of hybrid FMT-XCT reconstruction and cryosections between different time points of asthma model and control mouse. (a)–(c) 3-D rendering of mouse bone and lung based on XCT segmentation and fluorescence signal reconstructed from FMT-XCT. (a) Control mouse, (b) 6 weeks DRA-sensitized with ProSense680, (c) 9 weeks DRA challenged with ProSense680. (d) and (e) 3-D rendering of mouse lung based on color cryoslicing images and fluorescence signal from corresponding fluorescent cryosections. (d) Control mouse, (e) 6 weeks DRA-sensitized with ProSense680, (f) 9 weeks DRA challenged with ProSense680. Coordinate systems are designated by D (dorsal), V (ventral), Cr (cranial), Cd (caudal), L (left), and R (right). 3-D rendering was implemented using AMIRA software.

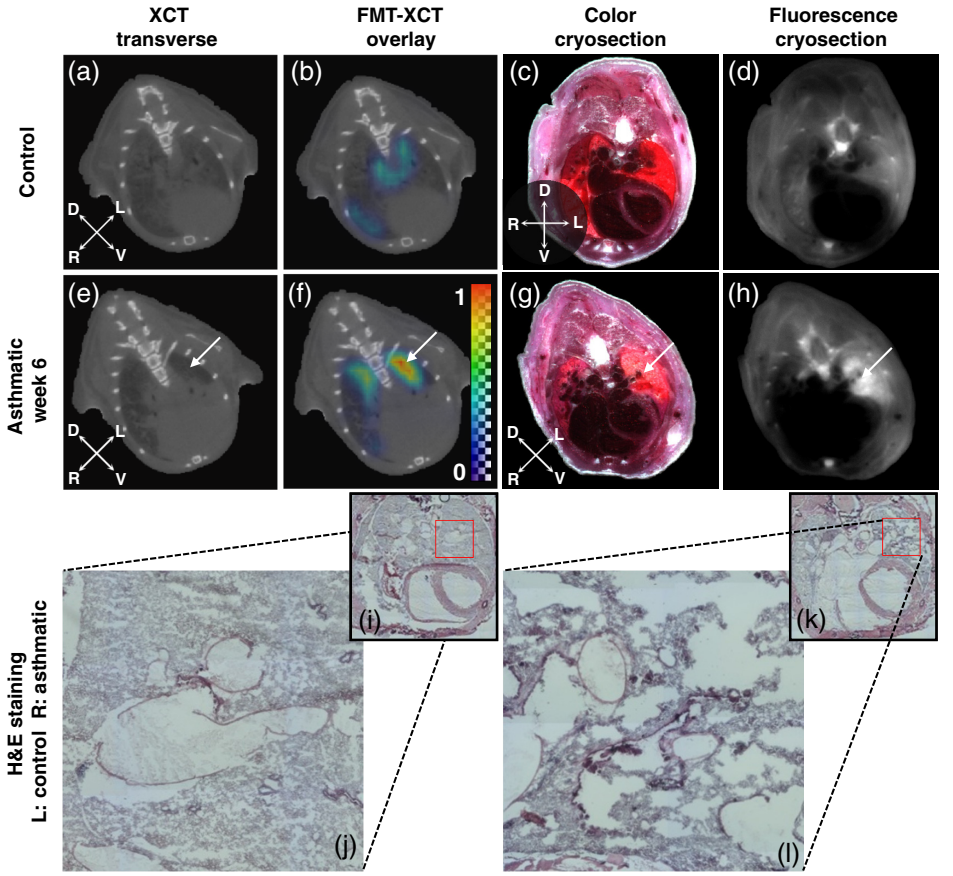

Fig. 4 Representative slice comparison of FMT-XCT reconstruction, cryoslicing image, and H&E staining in week 12 using MMPSense680 as the fluorescent agent. (a)–(d) Images obtained from different imaging modalities from same slice of the control mouse. (a) XCT transverse plane, (b) transverse slice of FMT reconstruction overlaid on XCT slice, (c) cryoslicing color image, (d) transverse-normalized fluorescent cryosection. (e)–(h) Images obtained from different imaging modalities from the same slice of the asthma model at a time point of 12 weeks (with 3 weeks rest after last DRA treatment in week 9). (e) XCT transverse plane, (f) transverse slice of FMT reconstruction overlaid on XCT slice, (g) cryoslicing color image, (h) transverse-normalized fluorescent cryosection for validation of FMT reconstruction. (i) and (j) H&E staining result of control mouse. (i) Whole sample slide. Enlarged view (j) represents the red rectangular region in (i). (k) and (l) H&E staining result of asthmatic mouse. (k) Whole sample slide. Enlarged view (l) represents the red rectangular region in (k). White arrows indicate the inflammatory and remodeling asthma region. Coordinate systems are designated by D (dorsal), V (ventral), L (left), and R (right).

fluorescence imaging to localize and identify asthma. On the other hand, Figs. 4(b) and 4(d) do not show a rise in fluorescence distribution using the control mouse treated with saline, confirming that fluorescence imaging has the capability to identify asthmatic conditions with very high sensitivity. Comparing the histological findings of the control mouse in Figs. 4(i) and 4(j) with the histology results of the DRA mouse in Figs. 4(k) and 4(l) indicates clear chronic lung morphologic damage. Figures 4(l) indicates that inflammation was found in the central area with immune cell accumulation and lymphocyte aggregation. Furthermore, lung remodeling can be observed in these mice, with an enlarged air space in the alveoli septum and loss of the lung structures. This obstructive lung disease was also clearly noticeable in our FMT-XCT reconstructions.

3.3 *Statistical Analysis*

In order to precisely assess the imaging capability of the hybrid FMT-XCT imaging system for evaluation of asthma-related inflammation severity, a quantitative assessment of *in vivo* FMT-XCT reconstructions versus corresponding *ex vivo* cryoslicing images was performed. The statistical analysis included evaluation of all the 16 mice used for this study. On the one hand, for the ProSense680 group, three control mice (one control mouse with 6 weeks saline treatment and two control mice with 9 weeks saline treatment), three mice with 6 weeks DRA challenge, and four mice with 9 weeks DRA challenge were used in total. On the other hand, for the MMPSense680 group, two control mice (9 weeks saline treatment and 3 weeks rest) and four asthmatic mice (9 weeks DRA treatment and 3 weeks rest) were imaged and analyzed.

Figure 5(a) shows the inflammation severity evaluation; the bar plot indicates the computed mean values of fluorescence intensity from *ex vivo* cryosections. The average values were computed at different time points using ProSense680 and MMPSense680 as fluorescent agents. A 58% increase of mean fluorescence intensity value was observed while comparing the mice treated with ProSense680 after 6 weeks of challenge with

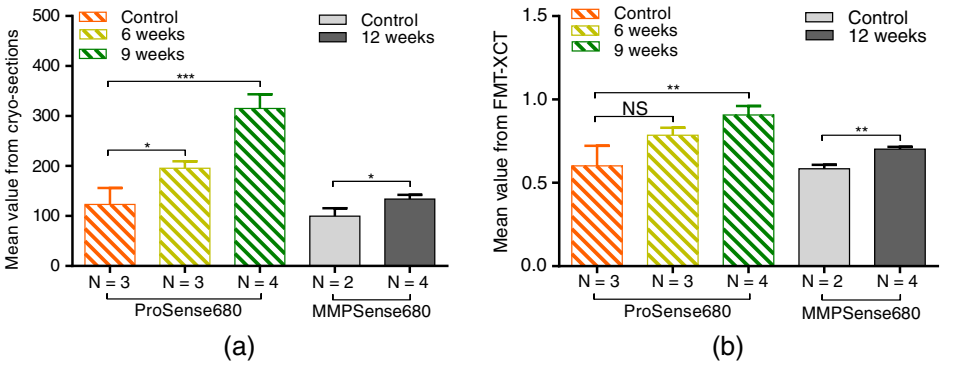

Fig. 5 Bar plots [mean ± standard error of the mean (SEM)] showing different inflammation and remodeling severity. The mean value is computed for the FMT-XCT reconstructions and the cryosection intensities for a DRA-challenged mice and a control group at different time points of the protocol. Colored bars depict the mice with ProSense680 at week 6 and week 9; gray ones show mice with MMPSense680 at week 12. (a) Bar plot shows the mean intensity values of cryoslicing. (b) Bar plot showing mean values reconstructed results from FMT-XCT. Asterisks indicate statistical significance using Student's *t*-test ($*p < 0.05$; $**p < 0.01$; $***p < 0.001$; NS, nonsignificant).

the control mice. On the other hand, a 155% increase was observed in asthmatic mice at week 9, resulting in a significant difference when compared to the mean values of fluorescence signal measured in the control mice. Note that a 61% increase was observed in asthmatic mice at week 9 compared to the asthmatic mice at week 6, indicating the capability of staging the asthmatic condition. In the MMPSense680 group, at 12 weeks (i.e., 3 weeks rest after the last DRA treatment in week 9), the asthma model showed a 34% increase relative to the corresponding saline-treated control group. Similar to the cryoslicing imaging, the average values were computed to evaluate the hybrid FMT-XCT imaging performance. The performance of FMT-XCT with ProSense680 as the fluorescence agent showed a 31% increase at week 6 and a 51% increase at week 9 compared to the control mice. Note that a 15% increase was observed in asthmatic mice at week 9 compared to the asthmatic mice at week 6. After 3 weeks rest in the MMPSense680 group, the asthmatic mice showed a 31% rise over the control group. All these increasing tendencies of FMT-XCT quantification correlated very well with *ex vivo* cryosection results.

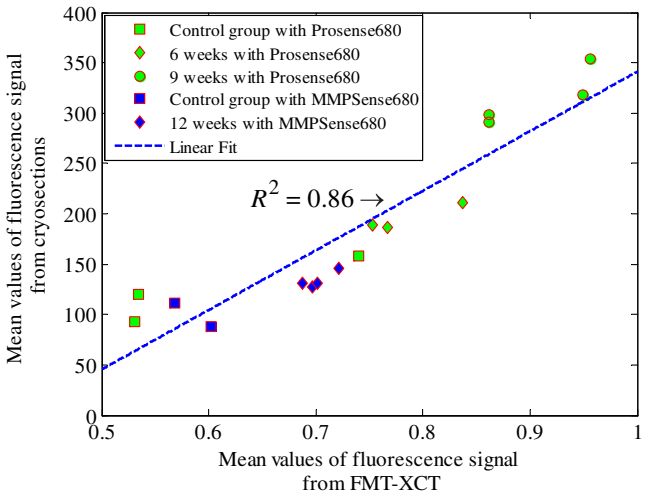

Fig. 6 Linear fit of mean value of the fluorescence signal from cryosection images, plotted against the FMT-XCT findings for all 16 mice studied.

FMT-XCT quantification results showed great consistency with *ex vivo* validation numbers. Figure 6 plots the mean fluorescence values obtained from the cryoslicing analysis against the corresponding values obtained with FMT-XCT. The mean values for the week-9 mice are higher compared to week-6 mice (ProSense 680), indicating that continued exposure to allergens increases the inflammatory burden in the lung.

4 Discussion

Noninvasive imaging techniques are increasingly considered in biomedical research and can lead to important insights on disease development on the same mouse model. However, while nuclear imaging methods can resolve biological contrast, they are limited by the short-lived radio-isotopes and the use of ionizing radiation, prohibiting repeated experiments on the same animal. FMT-XCT was investigated herein as an alternative imaging modality to nuclear methods for asthma research. The investigation focused on resolving cathepsins, a biomarker of eosinophil activity, and MMPs implicated in airway remodeling and inflammation.

Different studies have established the ability to utilize near-infrared fluorescent labels to resolve pulmonary inflammation and remodeling in COPD or asthma models.[25,26,28] Of particular importance herein was to interrogate the merits of hybrid 360-deg projection FMT-XCT and examine the image fidelity and quantification achieved as contrasted to fluorescence cryoslicing images, employed herein as an imaging gold standard. Since the selection of reconstruction parameters may alter the image parameters, we consistently employed the same parameter set for all mice scanned in this study, including estimates of the absorption coefficient and the scattering coefficient for different organs, which were based on previous literature estimates.[35]

FMT-XCT enabled the noninvasive study of DRA-based asthma responses at different time points. The *in vivo* results are consistent with previously established *ex vivo* observations of increases in eosinophil, mucus glycoproteins, α-smooth muscle actin, and collagenous fibers in the DRA asthmatic model 3 weeks after last challenge.[15] FMT-XCT resolved elevated fluorescence intensity in the lung region of the asthmatic mouse, showing increased cathepsin and MMP expression, further confirmed by *ex vivo* cryoslicing images. At the 12–week time point, the histological image of the DRA

model confirms the asthmatic inflammation and remodeling features.

Differences were observed between the fluorescence values obtained using the cathepsin-sensitive versus the MMP-sensitive probes. Overall, cathepsin-related signals were stronger and demonstrated higher relative increase compared to control mean fluorescence values. Using single activatable probes, it is not possible to distinguish between delivery and activation rate versus true enzyme concentration. However, dual wavelength methods[28] have been suggested to accurately quantify target concentration. With the establishment of FMT-XCT herein as a potent tool for asthma research, a next step would be the use of multiwavelength FMT-XCT to establish internal controls and offer more precise insights into the underlying biology. A secondary limitation herein was that the protease agents employed are sensitive to a profile of enzymes which may accumulate in both the inflammation region and remodeling region, so these processes cannot be explicitly differentiated herein. However, with increasing knowledge of available targets, a panel of agents more specific to individual processes may be foreseen in future applications of the technology.

The study confirmed the basic feasibility and elucidated the performance merits of FMT-XCT in asthma research. Remaining technology challenges are associated with the home-built nature of the FMT-XCT system, which utilized slow scanning machinery that resulted in data acquisition times of up to 1.5 h per mouse for a 3-D lung reconstruction. Optimization of scanning hardware and data acquisition protocols are possible[41,42] and would be necessary in the future to make the FMT-XCT application more practical for increasing the throughput ability. The use of graphic processing units[43,44] and of XCT contrast enhancement techniques such as phase contrast CT[36] or contrast agents that can improve the tissue contrast and accelerate tissue segmentation processes are necessary for the incorporation of XCT priors into the FMT inverse problem.[31]

Acknowledgments

This project has received funding from the European Union Project FMT-XCT (FP7 HEALTH, Contract 201792) and from the Deutsche Forschungsgemeinschaft, Germany (Leibniz Prize 2013; NT 3/10-1).

References

1. W. W. Busse and R. F. Lemanske Jr., "Asthma," *N. Engl. J. Med.* **344**(5), 350–362 (2001).
2. R. M. Locksley, "Asthma and allergic inflammation," *Cell* **140**(6), 777–783 (2010).
3. P. J. Barnes, "Immunology of asthma and chronic obstructive pulmonary disease," *Nat. Rev. Immunol.* **8**(3), 183–192 (2008).
4. J. V. Fahy, D. B. Corry, and H. A. Boushey, "Airway inflammation and remodeling in asthma," *Curr. Opin. Pulmonary Med.* **6**(1), 15–20 (2000).
5. P. C. Fulkerson, C. A. Fischetti, and M. E. Rothenberg, "Eosinophils and CCR3 regulate interleukin-13 transgene-induced pulmonary remodeling," *Am. J. Pathol.* **169**(6), 2117–2126 (2006).
6. T. Zheng et al., "Inducible targeting of IL-13 to the adult lung causes matrix metalloproteinase- and cathepsin-dependent emphysema," *J. Clin. Invest.* **106**(9), 1081 (2000).
7. H. Korideck and J. D. Peterson, "Noninvasive quantitative tomography of the therapeutic response to dexamethasone in ovalbumin-induced murine asthma," *J. Pharmacol. Exp. Ther.* **329**(3), 882–889 (2009).
8. C. Bergeron, M. K. Tulic, and Q. Hamid, "Airway remodelling in asthma: from benchside to clinical practice," *Can. Respir. J.* **17**(4), e85 (2010).
9. K. Górska et al., "Relationship between airway inflammation and remodeling in patients with asthma and chronic obstructive pulmonary disease," *Eur. J. Med. Res.* **14**(Suppl. 4), 90–96 (2009).
10. V. Lagente and E. Boichot, *Matrix Metalloproteinases in Tissue Remodelling and Inflammation*, Springer Science & Business Media, Switzerland (2008).
11. V. Lagente et al., "Role of matrix metalloproteinases in the development of airway inflammation and remodeling," *Braz. J. Med. Biol. Res.* **38**(10), 1521–1530 (2005).
12. J. J. Atkinson and R. M. Senior, "Matrix metalloproteinase-9 in lung remodeling," *Am. J. Respir. Cell Mol. Biol.* **28**(1), 12–24 (2003).
13. A. T. Nials and S. Uddin, "Mouse models of allergic asthma: acute and chronic allergen challenge," *Dis. Models Mech.* **1**(4–5), 213–220 (2008).
14. F. K. Swirski et al., "Chronic exposure to innocuous antigen in sensitized mice leads to suppressed airway eosinophilia that is reversed by granulocyte macrophage colony-stimulating factor," *J. Immunol.* **169**(7), 3499–3506 (2002).
15. N. Goplen et al., "Combined sensitization of mice to extracts of dust mite, ragweed, and *Aspergillus* species breaks through tolerance and establishes chronic features of asthma," *J. Allergy Clin. Immunol.* **123**(4), 925–932 (2009).
16. K. Jannasch, J. Missbach-Guentner, and F. Alves, "Using *in vivo* imaging for asthma," *Drug Discovery Today: Dis. Models* **6**(4), 129–135 (2010).
17. M. R. Miller et al., "Standardisation of spirometry," *Eur. Respir. J.* **26**(2), 319–338 (2005).
18. A. Schneider et al., "Diagnostic accuracy of spirometry in primary care," *BMC Pulm. Med.* **9**(1), 31 (2009).
19. M. Lederlin et al., "*In vivo* micro-CT assessment of airway remodeling in a flexible OVA-sensitized murine model of asthma," *PLoS One* **7**(10), e48493 (2012).
20. S. H. Paik et al., "A quantitative study of airway changes on micro-CT in a mouse asthma model: comparison with histopathological findings," *Allergy Asthma Immunol. Res.* **6**(1), 75–82 (2014).
21. M. Lederlin et al., "Airway remodeling in a mouse asthma model assessed by *in-vivo* respiratory-gated micro-computed tomography," *Eur. Radiol.* **20**(1), 128–137 (2010).
22. X. Artaechevarria et al., "Longitudinal study of a mouse model of chronic pulmonary inflammation using breath hold gated micro-CT," *Eur. Radiol.* **20**(11), 2600–2608 (2010).
23. H. Jones et al., "*In vivo* assessment of lung inflammatory cell activity in patients with COPD and asthma," *Eur. Respir. J.* **21**(4), 567–573 (2003).
24. S. R. Cherry and S. S. Gambhir, "Use of positron emission tomography in animal research," *ILAR J.* **42**(3), 219–232 (2001).
25. V. Ntziachristos et al., "Looking and listening to light: the evolution of whole-body photonic imaging," *Nat. Biotechnol.* **23**(3), 313–320 (2005).
26. V. Cortez-Retamozo et al., "Real-time assessment of inflammation and treatment response in a mouse model of allergic airway inflammation," *J. Clin. Invest.* **118**(12), 4058 (2008).
27. H. Korideck and J. D. Peterson, "Noninvasive, *in vivo* quantification of asthma severity using fluorescence molecular tomography," *Nat. Methods Appl. Notes* **5** (2008).
28. J. Haller et al., "Visualization of pulmonary inflammation using noninvasive fluorescence molecular imaging," *J. Appl. Physiol.* **104**(3), 795–802 (2008).
29. R. L. Barbour et al., "MRI-guided optical tomography: prospects and computation for a new imaging method," *Comput. Sci. Eng.* **2**(4), 63–77 (1995).
30. S. R. Arridge and J. C. Hebden, "Optical imaging in medicine: II. Modelling and reconstruction," *Phys. Med. Biol.* **42**(5), 841 (1997).
31. A. Ale et al., "FMT-XCT: *in vivo* animal studies with hybrid fluorescence molecular tomography-x-ray computed tomography," *Nat. Methods* **9**(6), 615–620 (2012).
32. K. Radrich et al., "Limited-projection-angle hybrid fluorescence molecular tomography of multiple molecules," *J. Biomed. Opt.* **19**(4), 046016 (2014).

33. P. Mohajerani et al., "Optical and optoacoustic model-based tomography: theory and current challenges for deep tissue imaging of optical contrast," *IEEE Signal Process Mag.* **32**(1), 88–100 (2015).
34. Y. Lin et al., "Quantitative fluorescence tomography with functional and structural *a priori* information," *Appl. Opt.* **48**(7), 1328–1336 (2009).
35. D. Hyde et al., "Performance dependence of hybrid x-ray computed tomography/fluorescence molecular tomography on the optical forward problem," *J. Opt. Soc. Am. A* **26**(4), 919–923 (2009).
36. P. Mohajerani et al., "FMT-PCCT: hybrid fluorescence molecular tomography-x-ray phase-contrast CT imaging of mouse models," *IEEE Trans. Med. Imaging* **33**(7), 1434–1446 (2014).
37. V. Ermolayev et al., "Early recognition of lung cancer by integrin targeted imaging in K–ras mouse model," *Int. J. Cancer* **137**(5), 1107–1118 (2015).
38. C. C. Paige and M. A. Saunders, "LSQR: an algorithm for sparse linear equations and sparse least squares," *ACM Trans. Math. Software* **8**(1), 43–71 (1982).
39. A. Sarantopoulos, G. Themelis, and V. Ntziachristos, "Imaging the bio-distribution of fluorescent probes using multispectral epi-illumination cryoslicing imaging," *Mol. Imaging Biol.* **13**(5), 874–885 (2011).
40. B. R. Troen, "The role of cathepsin K in normal bone resorption," *Drug News Perspect.* **17**(1), 19–28 (2004).
41. E. E. Graves et al., "Singular-value analysis and optimization of experimental parameters in fluorescence molecular tomography," *J. Opt. Soc. Am. A* **21**(2), 231–241 (2004).
42. A. Jin et al., "Preconditioning of the fluorescence diffuse optical tomography sensing matrix based on compressive sensing," *Opt. Lett.* **37**(20), 4326–4328 (2012).
43. X. Wang et al., "Acceleration of early-photon fluorescence molecular tomography with graphics processing units," *Comput. Math. Methods Med.* **2013**, 1–9 (2013).
44. J. Prakash et al., "Accelerating frequency-domain diffuse optical tomographic image reconstruction using graphics processing units," *J. Biomed. Opt.* **15**(6), 066009 (2010).

Xiaopeng Ma is currently a PhD student in the Institute for Biological and Medical Imaging at Technische Universität München and Helmholtz Zentrum München, Munich, Germany. He received his BS degree in electronic science and technology in 2008 and later received his MSc degree in electrical engineering in 2011, both from Xidian University, China. His current research interests are fluorescence molecular tomography, x-ray computed tomography, and *in vivo* biomedical imaging applications.

Biographies for the other authors are not available.